CRYSTAL GROWTH & DESIGN

Article

Cite This: Cryst. Growth Des. 2018, 18, 5556−5563

pubs.acs.org/crystal

Capturing Elusive Polymorphs of Curcumin: A Structural Characterization and Computational Study

Maria A. Matlinska,[†] Roderick E. Wasylishen,*[,†] Guy M. Bernard,[†] Victor V. Terskikh,[‡] Andreas Brinkmann,[§] and Vladimir K. Michaelis[†]

[†]Department of Chemistry, University of Alberta, Edmonton, Alberta T6G 2G2, Canada

[‡]Department of Chemistry, University of Ottawa, Ottawa, Ontario K1N 6N5, Canada

[§]Metrology, National Research Council Canada, 1200 Montreal Road, Ottawa, Ontario K1A 0R6, Canada

Supporting Information

ABSTRACT: Curcumin, a compound derived from the herb turmeric, has gained considerable attention because of its purported pharmacological activity, but its poor water solubility and low bioavailability impedes its therapeutic potential. In addition to the frequently studied curcumin polymorph, referred to as form I, another polymorph with enhanced water solubility, referred to as form II, or red curcumin, has also been reported. We discuss experimental challenges in isolating the red curcumin polymorph. In the course of our studies, we were unable to obtain a third reported polymorph, form III. We redetermined crystal structures of forms I and II of curcumin and present ^{13}C and ^{1}H solid-state nuclear magnetic resonance (NMR) spectra for these two forms, as well as $^{13}C-^{1}H$ two-dimensional heteronuclear correlation (HETCOR) data. The experimental ^{1}H and ^{13}C nuclear magnetic resonance (NMR) chemical shifts are compared with GIPAW density functional theory values computed using CASTEP. Our research illustrates the utility of NMR spectroscopy in characterization of polymorphism in bulk samples.

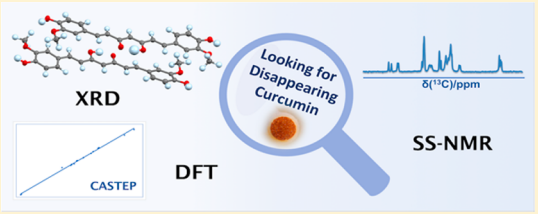

INTRODUCTION

Curcumin, 1,7-bis(4-hydroxy-3-methoxyphenyl)-1,6-heptadiene-3,5-dione (Scheme 1), is a natural product found in turmeric (*Curcuma longa*), a plant of the ginger family.[1−5] Turmeric has been harvested and used in traditional Indian cooking and medicine for centuries.[1,3] Especially interesting components of turmeric are the curcuminoids, in particular curcumin, which are responsible for the orange color of turmeric.[4,5] Curcumin has been of interest to the medical community because of its reported anti-inflammatory, antioxidant, and anticancer properties.[1−11] It has been also shown to break down β-amyloid fiber aggregates in the brain that are the hallmark of neurodegenerative diseases, such as Alzheimer's disease.[1,4,7] However, the methodology of many medicinal studies of curcumin is controversial, and their reliability are currently under intense scrutiny by the scientific community.[12−16] A major limitation of using curcumin as a pharmaceutical is its poor water solubility and hence low bioavailability.[17] Various approaches have been undertaken to enhance curcumin's bioavailability, e.g., microfluidic fabrication of cationic nanoparticles,[18] preparing curcumin-conjugated gold nanoparticles,[19] curcumin-resorcinol and curcumin-pyrogallol cocrystals,[20] and curcumin nanosuspensions.[21] Also, it has been suggested that one or both of the phenolic hydrogens can be replaced by a hydrophilic group such as the phosphonium cation.[22] More recently, the latter curcumin derivative has been used to prepare a cobalt(III) complex that is claimed to display a remarkable photodynamic therapy effect.[23] As well, the group of Chakravarty has recently synthesized vanadium(IV) complexes of curcumin.[24]

Scheme 1. Structure of the Diketo Form of Curcumin

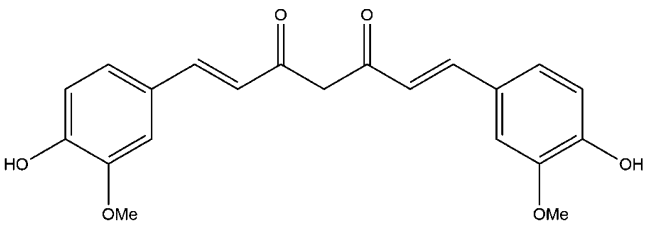

The solid-state structure of curcumin in the monoclinic space group $P2/n$ was first reported in 1982 by Tønessen and co-workers,[25] and later by Parimita et al.[26] and by Sanphui and co-workers.[27] More recently, the structure was determined via synchrotron powder X-ray diffraction (XRD).[28] Two additional polymorphs of curcumin have also been reported by Sanphui et al.[27] The two new polymorphs, referred to as forms II and III, belong to the orthorhombic space groups $Pca2_1$ and $Pbca$, respectively.[27] The unit cell of form II contains two crystallographically non-equivalent molecules while all eight molecules in the unit cell of form III were reported to be

Received: June 5, 2018
Revised: July 19, 2018
Published: August 9, 2018

DOI: 10.1021/acs.cgd.8b00859
Cryst. Growth Des. 2018, 18, 5556−5563

crystallographically equivalent.[27] In 2012, Parameswari et al.[29] also reported the structure of the orthorhombic form, $Pca2_1$ (i.e., form II) at 100 K; the crystals were obtained from propan-2-ol. Both forms I and II of curcumin exist in the solid state as keto−enol tautomers (see Scheme 2). As well, the keto−enol tautomer is the only tautomer detected in NMR studies of curcumin in solvents with a wide range of dielectric constants[30] (e.g., chloroform, acetone, methanol, DMSO, and D_2O/DMSO mixtures).[31] Apparently the form II polymorph of curcumin has a higher aqueous dissolution rate in a 40% ethanol/water mixture than that for the common and most studied crystalline polymorph (form I).[27] In a 2015 report, Rasmuson et al.[32] reported the preparation of two polymorphs of curcumin: form I was prepared readily, and with careful handling a second polymorph was obtained; on the basis of powder XRD, the authors concluded that this was form III as previously described by Sanphui et al.,[27] but they acknowledge that the powder patterns for forms II and III are expected to be similar; they were unable to obtain Form II. A year later, Rasmuson[33] and co-workers discussed the purification of curcumin and, in this case, reported forms I and II. Thorat and Dalvi obtained solid form III, but only with the use of ultrasound.[34]

Scheme 2. Molecular Structures for Form I and for Molecules A and B of Form II of Curcumin[a]

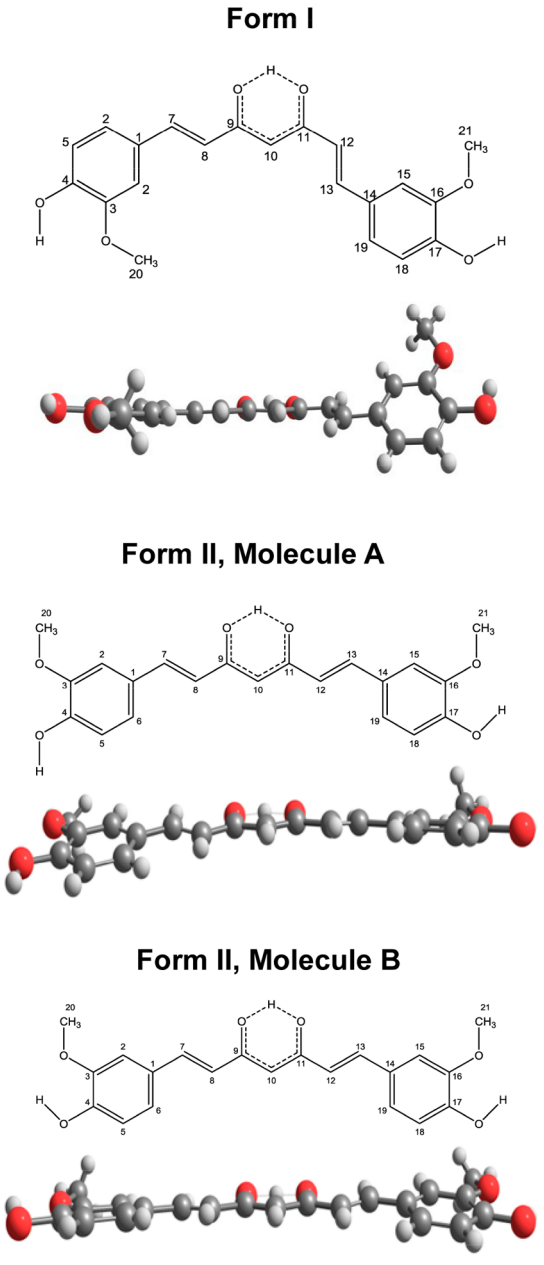

[a]Red = oxygen, light grey = hydrogen, and dark grey = carbon. The atom labeling used in the text is shown, as well as a view of each molecule approximately perpendicular to the page to illustrate how they deviate from planarity.

Although solid-state ^{13}C NMR spectroscopy is ideally suited to study polymorphism,[35−43] the only study of curcumin polymorphs via solid-state NMR is that of Sanphui et al.[27] Noting a discrepancy between their reported NMR data for form III and their corresponding single-crystal X-ray crystallography data,[27] and suspecting a misassignment of some ^{13}C MAS NMR resonances by these and other authors,[44] we have obtained high-resolution solid-state ^{1}H and ^{13}C NMR spectra of the two most studied curcumin polymorphs (forms I and II), redetermined their single-crystal structures, and performed GIPAW (gauge including projector augmented waves) density functional theory (DFT) magnetic shielding calculations for forms II and III; results are compared with those obtained from our earlier study of form I.[45] We propose assignments of the ^{13}C and ^{1}H NMR spectra for form II. In the course of our studies, we found that the preparation of form II is not straightforward, but once formed, is stable for months.

EXPERIMENTAL SECTION

Sample Preparation. Form I of curcumin was obtained from Sigma-Aldrich (St. Louis, MO) and recrystallized by dissolving the sample in warm isopropyl alcohol, allowing it to cool, filtering the resulting crystals and drying on a vacuum line.

Form II was obtained in a two-step crystallization from 95% ethanol. Solid curcumin (200 mg) was dissolved in a minimum amount of hot or boiling solvent (temperature either 2−3 °C below the boiling point or at the boiling point). The solution was then rapidly cooled to 7−9 °C in an ice−water bath and suction-filtered using a Buchner funnel with filter paper of medium porosity and a slow flow rate. The filtrate was then collected and stored at 3−4 °C in glass containers secured with perforated parafilm until enough solid crystallized to repeat the purification procedure. The shortest time at which solid form II crystallized from ethanol was 72 h. The volume of hot solvent and the time required to dissolve the solid increased with each crystallization step (9.6 mL of ethanol in step one, 20.0 mL in step two, similar for other solvents).

Crystallization from all solvents used by Sanphui et al.[27] was attempted, but only ethanol as a solvent yielded the desired polymorph on one occasion; see Table S7 in Supporting Information (SI) for details on several recrystallization attempts. Co-crystallization with 4-hydroxypyridine and 4,6-dihydroxy-5-nitropyrimidine in ethanol, as described in the literature,[27] as well as seeding with a mixture of form I and form II crystals, similar to the method reported by Ukrainczyk et al.[33] was unsuccessful, yielding form I in all cases; due to technical limitations, we were unable to achieve the rigorous cooling rate control and conditions described by these authors. In summary, obtaining form II proved challenging; the difficulties with curcumin polymorphism have been discussed.[34] Such difficulties have been encountered for other compounds, and the term "disappearing polymorphs" has been appropriately used when describing this phenomenon.[46]

Initial screening for samples for solid-state NMR characterization was largely based on their color (red samples were believed to contain form II, whereas light orange was suspected to be mainly form I, as

DOI: 10.1021/acs.cgd.8b00859
Cryst. Growth Des. 2018, 18, 5556−5563

described by Liu et al.),[32] but we found that characterization by solid-state NMR spectroscopy or single-crystal X-ray crystallography is essential to ascertain that the desired polymorph has been obtained. The form II of curcumin is stable for at least 15 months when stored in a sealed container, as confirmed by performing periodic ^{1}H and ^{13}C CP/MAS experiments.

X-ray Crystallography. Single-crystal data of form II of curcumin were collected at −100 °C on a Bruker D8/APEX II CCD diffractometer with a Cu K_α radiation source, λ = 1.54178 Å. Programs for diffractometer operation, data collection, data reduction, and absorption correction were those supplied by Bruker. The structure was solved by the intrinsic phasing SHELXT-2014 method[47] and refined with SHELXL-2014.[48]

Solid-State Nuclear Magnetic Resonance Spectroscopy. Solid-state ^{13}C NMR spectra were obtained at 7.05 T using a Bruker Avance 300 NMR spectrometer operating at 75.5 MHz for ^{13}C, with a Bruker 4 mm double-resonance magic-angle spinning (MAS) probe, in a cross-polarization (CP) experiment[49] with a contact time of 3.5 ms, a recycle delay of 5 s and a MAS frequency of 11 kHz. A 4.0 μs 90° ^{1}H pulse and a two-pulse phase-modulated (TPPM)[50] decoupling field of 62.5 kHz was used to acquire all solid-state ^{13}C NMR spectra, which were referenced to TMS (δ_{iso} = 0 ppm) by setting the high-frequency peak of adamantane to 38.56 ppm.[51] ^{13}C NMR spectra for a MAS sample of bis-demethoxycurcumin were acquired under similar conditions at 11.75 T with a spinning frequency of 12.5 kHz.

Two-dimensional ^{13}C−^{1}H HETCOR NMR spectra were acquired at 21.1 T at the National Ultrahigh-field NMR Facility for Solids in Ottawa, Canada, on a Bruker Avance II 900 NMR spectrometer. These were obtained using a Bruker 4 mm HCN MAS probe, with a contact time of 0.25 (form I) or 0.5 ms (form II), a recycle delay of 10 or 20 s, respectively, for forms I and II, and a MAS frequency of 18 kHz; spectra were acquired with 32 t_1 increments of 18.88 μs. The spectrum for form I was acquired in less than 24 h by coadding 268 transients for each slice, but the limited sample amount (≈15 mg) and the presence of two molecules in the asymmetric unit for form II meant that 640 coadded transients per slice were required for this sample; combined with its longer ^{1}H T_1 relaxation time, a total of 5 days was required to acquire the spectrum. One-dimensional solid-state CP/MAS ^{13}C NMR spectra were obtained on this instrument using similar conditions as for the HETCOR experiment, but with a contact time of 5.0 ms. Solid-state ^{1}H NMR spectra were acquired on this instrument with a Bruker 1.3 mm H/X MAS probe using a rotor-synchronized echo pulse sequence (i.e., 90°−τ−90°−τ−acquire, where τ is the interpulse delay) with a recycle delay of 30 s and a 90° pulse of 2.0 μs, at a MAS frequency of 50 kHz. The ^{1}H and ^{13}C spectra were referenced to TMS (δ_{iso}= 0 ppm) by setting the isotropic ^{1}H peak of adamantane to 1.8 ppm[52] and the isotropic ^{13}C carbonyl peak of glycine to 176.5 ppm.[53]

GIPAW DFT Calculations. GIPAW DFT calculations were performed using the Cambridge Sequential Total Energy Package (CASTEP) code (version 2017), which uses a plane-wave pseudopotential approach.[54] The generalized gradient approximation with the Perdew−Burke−Ernzerhof exchange correlation functional was used.[55,56] The crystal structure of curcumin form II determined by X-ray crystallography as described above was used as the starting point for the geometry optimization, for which the Broyden−Fletcher−Goldfarb−Shanno (BFGS) algorithm,[57−61] on-the-fly generation (OTFG) ultrasoft pseudopotentials (version 80), a cutoff energy of 571.4 eV, and a 1 × 2 × 1 k-point grid were chosen. Subsequently, NMR parameters were computed with the NMR module within CASTEP employing OTFG pseudopotentials (version 00), a cutoff energy of 550 eV, and a 1 × 2 × 1 k-point grid. Calculated isotropic magnetic shielding values were converted to calculated isotropic chemical shift values as follows: for hydrogen, δ/ppm (calc.) = 29.0/ppm − σ/ppm (calc.), and for carbon, δ/ppm (calc.) = 170.4/ppm − σ/ppm (calc.).[45]

RESULTS AND DISCUSSION

Single-Crystal X-ray Diffraction: Structural Differences between Forms I and II of Curcumin. Knowledge of the solid-state crystal structures of compounds under investigation aides greatly in the analysis of the solid-state ^{13}C NMR spectra. Thus, to ascertain that the desired polymorphs of curcumin had been obtained, single-crystal X-ray diffraction data were obtained for both forms I and II; see SI Tables S1−S4 and Figures S1 and S2 for a detailed listing of the parameters derived from these analyses. We have carefully compared our results with reported structures for forms I[25−28] and II,[27,29] finding only minor differences. Unless otherwise specified, the single-crystal X-ray data obtained in our lab will be presented in the discussion below.

Single-crystal X-ray diffraction data reveals several distinguishing features between forms I and II of curcumin: form I is monoclinic with a single crystallographically distinct molecule within its asymmetric unit, while form II is orthorhombic with two crystallographically distinct molecules, designated as molecules A and B, in its asymmetric unit (see Scheme 2). A notable feature for form I is the arrangement of its C10−C11−C12−C13 fragment (Scheme 2), with C13 oriented cis to C10. In addition, the C12−C13−C14−C15 atoms diverge from the near planarity found for atoms C1 through C11 such that the phenyl moiety bonded to C13 forms an angle of approximately 43° with this plane. In contrast, form II has an all-*trans* arrangement of the C10−C11−C12−C13 fragments of both molecules A and B, and there are only minor deviations from planarity for these molecules. Applying a rotation of approximately 165° about the C11−C12 bond for form I results in the approximate arrangement observed for form II (Scheme 2). The planarity and all-trans configuration of the C7 through to C13 fragment of the form II polymorph is most likely responsible for its red color (bathochromic shift)[62] compared to the yellow-orange form I polymorph.[63,64] Note that dark red form I crystals have also been reported,[25] serving as a reminder that one should be cautious when characterizing compounds using subjective methods such as a visual inspection. When practical, instrumental analyses are preferred.

Of particular interest in interpreting the solid-state ^{1}H and ^{13}C NMR spectra of forms I and II is a comparison of the hydrogen-bonding interactions, also summarized in SI Tables S2 and S4. The strength of O···H···O hydrogen bonds is often related to the separation of the oxygen atoms of the hydrogen-bonded fragment of the molecule under consideration. In general, distances less than 2.5 Å are considered an indication of strong hydrogen bonds in which case the barrier between the zero-point energies (ZPE) of the two potential wells is comparable to the barrier between the two wells.[65−68] In contrast, if the O−O separations are in the 2.6 to 2.8 Å range,[68] the barrier between the two potential wells is generally significantly above the ZPE of each well and the hydrogen bonds are normally classified as moderate or weak.[68,69] The relationship between barrier height and ZPEs in the keto−enol fragment of 1,3-β-diketones is nicely illustrated in the study of McKenzie et al.[68] Another method of assessing the strength of hydrogen bonds in the keto−enol fragment of β-diketones is through the investigation of a possible interplay between a local resonance structure and hydrogen bonding (i.e., resonance-assisted hydrogen bonding or RAHB),[70−72] as illustrated in Figure S3. Delocalization in the enol-keto fragment is an indication of strong hydrogen bonding. In a

DOI: 10.1021/acs.cgd.8b00859
Cryst. Growth Des. 2018, 18, 5556−5563

fully delocalized symmetric system, the two C−O bond lengths and the two C−C bond lengths are equal. At the other extreme, where the keto−enol fragment consists of isolated C−O−H and C═O fragments, one may expect a significant difference between the C−O and the C−C bond lengths. For example, based on standard bond lengths proposed by J. A. Pople and D. L. Beveridge,[73] one expects the C−O bond length of a C═O bond to be 1.22 Å, while in the C−O−H fragment the C−O bond length would be approximately 1.36 Å. Note that these values are within experimental error of the C═O bond length determined for benzophenone, 1.23 Å,[74] and the C−O bond length in phenol, 1.374 Å.[75] Similarly, the C−C bond lengths in the O═C−C and O−C═C fragments are expected to be 1.46 and 1.34 Å, respectively. Thus, differences in these bond lengths (see Tables S5 and S6) are an indication of the hydrogen bond strength. See Section 2 of Supporting Information for a more detailed discussion of this analysis.

The molecules of form I exhibit three intramolecular hydrogen bonds: a strong intramolecular H-bond in the keto−enol fragment of the *β*-diketone fragment is expected with an O3−O4 separation of 2.456 Å, and both phenyl OH groups for this form participate in H-bonding with their adjacent methoxy groups with O−O separations of 2.674 and 2.700 Å. There also is one intermolecular H-bond involving one of the oxygen atoms of the keto−enol fragment and a phenyl OH group, with an O−O separation of 2.807 Å.

The bonding arrangements for the two molecules in the asymmetric unit of form II of curcumin differ slightly. Molecule A has two intramolecular H-bonds, the strongest being the one in the keto−enol fragment with an O−O separation of 2.530 Å, and a weaker one involving the phenyl OH and adjacent methoxy group, with an O−O separation of 2.714 Å. Note that the other phenyl OH group forms a moderately strong intermolecular H-bond with one of the oxygens of the keto−enol fragment in a neighboring molecule A, 2.633 Å (Figure S4). For isolated 2-methoxyphenol, quantum chemistry computations indicate that the conformation of the O−H *cis* to the methoxy oxygen is more stable than the *trans* conformation by 4.43 kcal mol^{-1} (18.5 kJ mol^{-1}).[76] Intramolecular OH···OMe hydrogen bonding in 2-methoxyphenol is also consistent with gas-phase electron diffraction experiments and quantum chemistry calculations.[77] These observations support the idea that the intermolecular hydrogen bond between the phenyl OH on C4A and the oxygen of the keto−enol fragment, specifically O3A, must be relatively strong. Molecule B of form II of curcumin has three intramolecular H-bonds, again the one in the keto−enol fragment, with an O−O separation of 2.501 Å, is the strongest while the other two involve the phenyl OH groups and adjacent methoxy oxygens analogous to that observed for form I, with O−O separations of 2.652 and 2.650 Å. In addition, there are also weaker intermolecular H-bonds. Note that although, on the basis of the O−O separation, the intramolecular hydrogen bonds for the keto−enol fragments of both molecules A and B are expected to be strong, this assessment nevertheless predicts that these hydrogen bonds will be weaker than the corresponding bond in form I, which has a significantly shorter O−O separation. Weaker hydrogen bonding in form II is also supported by the enol OH proton chemical shifts in the solid state.

Solid-State NMR Spectroscopy. Figures 1 and 2 illustrate ^{13}C and ^{1}H solid-state MAS NMR spectra of samples for forms I and II, respectively. The obvious difference in ^{13}C NMR spectra of forms I and II is that the number of resolved peaks observed for form II is greater than that for form I; since there are two molecules in the asymmetric unit for form II, there are, ignoring overlap, double the NMR peaks observed for form I, complicating the assignment of the spectrum. For example, four peaks are observed in the carbonyl region for form II, as expected. However, on the basis of this one-dimensional NMR spectrum, it is impossible to assign these peaks to either molecule A or B. Likewise, there are three peaks with an approximate 2:1:1 intensity ratio in the methyl region, as expected from a structure containing two distinctive molecules, each with two distinctive methoxy groups. The distinct carbonyl carbon and enolic ^{1}H NMR peaks for this sample suggest that an NMR correlation experiment may be instructive (*vide infra*).

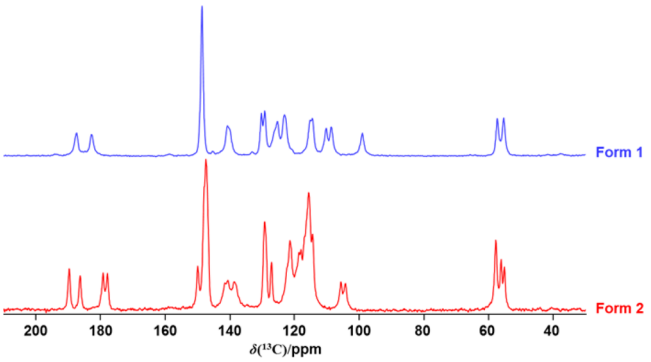

Figure 1. ^{13}C NMR spectra of forms I and II of solid curcumin, obtained with CP at 7.05 T with a magic-angle spinning frequency of 11 kHz.

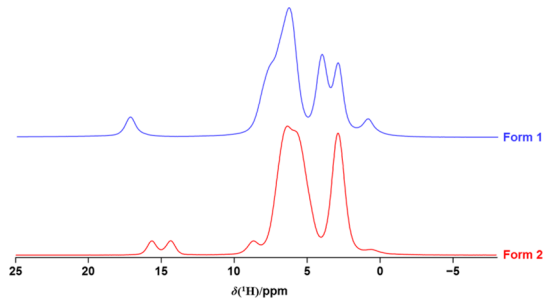

Figure 2. ^{1}H NMR spectra of forms I and II of solid curcumin acquired at 21.1 T with a magic-angle spinning frequency of 50 kHz.

Solid-state ^{1}H NMR spectroscopy may also provide information on the nature of hydrogen-bonded systems, with the ^{1}H chemical shift of the enolic proton increasing with increasing hydrogen bond strength.[67,78−85] That for form I is 16.8 ppm,[45] but the corresponding values for molecules A and B of curcumin in II are 14.5 and 15.7 ppm (Figure 2), suggesting a stronger hydrogen bond for the enolic proton of form I, consistent with the predictions based on O−O separations discussed above.

To further characterize the ^{13}C NMR spectrum for solid form II, a $^{13}C-^{1}H$ HETCOR spectrum was acquired at 21.1 T. The carbonyl region of that spectrum is shown in Figure 3, where it clearly indicates that the two inner carbonyl ^{13}C peaks are correlated with the less shielded of the two enolic ^{1}H nuclei. Unfortunately, there is insufficient resolution in the ^{1}H spectrum for form II to use a similar approach to distinguish between other ^{13}C peaks from molecules A and B (e.g., while

DOI: 10.1021/acs.cgd.8b00859
Cryst. Growth Des. 2018, 18, 5556−5563

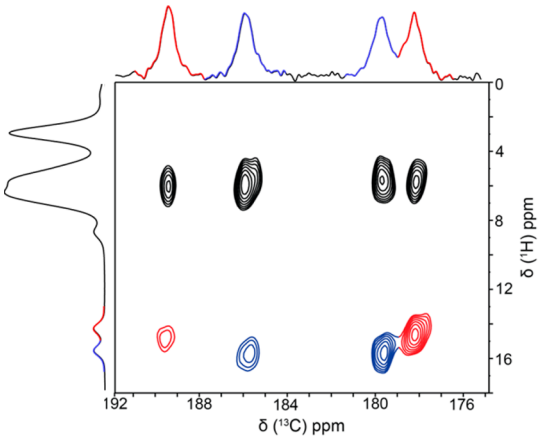

Figure 3. Carbonyl region of the $^{13}C-^{1}H$ HETCOR NMR spectrum for solid curcumin, form II, acquired at 21.1 T at an MAS frequency of 18 kHz. On the basis of the GIPAW DFT calculations, the blue inner two cross-peaks are from molecule A and the red outer two cross-peaks are from molecule B. The ^{1}H NMR chemical shifts of the enolic protons are 15.7 ppm (molecule A) and 14.5 ppm (molecule B). Note that the 1D spectra illustrated here were obtained in separate measurements with spinning frequencies of 50 kHz (^{1}H) and 18 kHz (^{13}C).

three peaks are resolved in the region of the methyl carbons, the corresponding ^{1}H peaks are not resolved; see Figure S5). Further information is required to assign ^{13}C NMR peaks to either molecule A or B; for this, we turn to computational results, discussed later.

While our single-crystal XRD data of curcumin form II discussed above are consistent with those obtained in earlier studies,[27,29] such is not the case for our solid-state ^{13}C NMR spectrum for form II. Our ^{13}C NMR spectrum for form II is completely different than that reported by Sanphui et al.[27] who reported ^{13}C NMR peaks in the 156−163 ppm region; however, we did not observe any peaks in this region. The authors assigned these peaks to C4 and C17 (Scheme 2), as did Zhao et al.[43] for form I. We only observed peaks in this region for spectra acquired for form I prior to sample recrystallization, indicating that these peaks arise from impurities. A solid-state ^{13}C NMR spectrum of a probable impurity, bisdemethoxycurcumin (BDMC), contains a peak at 160 ppm; also, ^{13}C NMR spectra for samples of BDMC and demethoxycurcumin (DMC) dissolved in various solvents contain a peak in the 159.7 to 160.5 ppm region.[86,87] Commercial curcumin contains significant amounts of DMC (≈17%) and BDMC (≈3%) impurities.[2]

The solid-state ^{13}C NMR spectrum of form III reported by Sanphui et al.[27] appears to contain approximately twice the number of peaks expected on the basis of the crystal structure,[27] which has one distinct molecule in the asymmetric unit. For example, there are four ^{13}C NMR peaks in the 175 to 190 ppm region rather than the two expected from the reported crystal structure. Observation of twice as many nonequivalent carbon centers as expected suggests either two distinct molecules in the unit cell, or a spectrum for a mixture of two or more compounds. These authors also reported a ^{13}C spectrum for form II, attributing the peak broadening to higher amorphous content compared with spectra for the other polymorphs; however, their reported chemical shifts[27] are inconsistent with our values.

DFT Calculation Results and Peak Assignment. GIPAW DFT calculations were undertaken to further assign ^{13}C and ^{1}H solid-state NMR spectra (Figures 1 and 2, respectively) of form II of curcumin. A plot of experimental vs computed ^{13}C chemical shifts is shown in Figure S6. The R^2 value of 0.997 for both molecules A and B indicates a strong positive correlation, with only one significant outlier, for the peak with an experimental value of approximately 105 ppm, corresponding to C10. The calculation results, summarized in Table S8, suggest that the two outer ^{13}C carbonyl peaks at 178.1 and 189.5 ppm are from molecule B, while the two inner peaks at 179.6 and 189.5 ppm are from molecule A. These results are consistent with the experimental $^{13}C-^{1}H$ HETCOR NMR spectrum discussed above. However, agreement between experiment and theory is not as good for the ^{1}H chemical shifts (see Table S8) probably due to the narrower range of chemical shifts for ^{1}H. For example, calculations suggest that molecule A, which contains the two inner carbonyl ^{13}C peaks, also contains the more shielded enolic ^{1}H, contradicting the $^{13}C-^{1}H$ HETCOR NMR results, which show that this proton is in the molecule with the two outer carbonyl peaks. In light of the better agreement between experimental and calculated ^{13}C chemical shifts, the error is thought to be in the calculated ^{1}H results, and thus, the least shielded enolic ^{1}H is assigned to molecule A. In a combined solid-state NMR and computational study of form I of curcumin and of dibenzoylmethane, Kong et al. considered the nonclassical enolic proton probability distribution caused by nuclear quantum effects,[45] concluding that a computational methodology that treats this proton as a static entity can lead to a failure of DFT results.[45] Finally, it is well-known that ^{1}H NMR chemical shifts of hydrogen-bonded O−H groups are strongly dependent on temperature[88−91] (i.e., vibrational averaging and detailed dynamics of the O−H moiety[92]).

CONCLUSIONS

Form II of curcumin has been prepared and its crystal structure confirmed by solid-state NMR spectroscopy and X-ray crystallography. Although the experimental procedure for obtaining red curcumin is not straightforward, once formed, it is stable for months under normal storage conditions. Based on ^{1}H, ^{13}C, and 2D $^{13}C-^{1}H$ HETCOR NMR results and on results obtained from single-crystal X-ray diffraction and from GIPAW DFT calculations, we have assigned the ^{13}C NMR peaks for form II of curcumin. We conclude that peaks in the 156−163 ppm region previously assigned to C4 and C17 are from impurities that can be removed through recrystallization. Our high-resolution ^{13}C NMR spectra for solid form II indicate that it is possible to obtain crystalline powder samples of this form through recrystallization. Finally, experimental $^{13}C-^{1}H$ HETCOR NMR results are consistent with GIPAW DFT calculations in assigning ^{13}C peaks to molecules A and B, but these calculations failed to predict the relative ^{1}H chemical shifts of the enol protons.

ASSOCIATED CONTENT

Supporting Information

The Supporting Information is available free of charge on the ACS Publications website at DOI: 10.1021/acs.cgd.8b00859.

Single-crystal X-ray diffraction, resonance assisted hydrogen bonding, and additional figures and tables (PDF)

DOI: 10.1021/acs.cgd.8b00859
Cryst. Growth Des. 2018, 18, 5556−5563

Accession Codes

CCDC 1847464−1847465 contain the supplementary crystallographic data for this paper. These data can be obtained free of charge via www.ccdc.cam.ac.uk/data_request/cif, or by emailing data_request@ccdc.cam.ac.uk, or by contacting The Cambridge Crystallographic Data Centre, 12 Union Road, Cambridge CB2 1EZ, UK; fax: +44 1223 336033.

AUTHOR INFORMATION

Corresponding Author

*Tel: +1-780-492-4336. E-mail: roderick.wasylishen@ualberta.ca.

ORCID

Roderick E. Wasylishen: 0000-0003-4150-3651
Guy M. Bernard: 0000-0003-1507-6705
Victor V. Terskikh: 0000-0003-1514-2610
Vladimir K. Michaelis: 0000-0002-6708-7660

Notes

The authors declare no competing financial interest.

ACKNOWLEDGMENTS

The Natural Sciences and Engineering Research Council (NSERC) of Canada and the University of Alberta are acknowledged for generous research support. Access to the 21.1 T NMR spectrometer was provided by the National Ultrahigh-Field NMR Facility for Solids (Ottawa, Canada), a national research facility funded by a consortium of Canadian universities and by an NSERC RTI grant, and supported by the National Research Council of Canada and Bruker BioSpin, managed by the University of Ottawa (http://nmr900.ca). MAM was partially supported by the Undergraduate Researcher Stipend provided by the University of Alberta Undergraduate Research Initiative, and by the Dr. R. Norman and Magda Kemeny Jones Summer Studentship. The authors thank Dr. Robert McDonald for obtaining single-crystal X-ray data and Dr. Michael Ferguson for helpful comments, Ms. Qichao Wu and Ms. Michelle Ha for their assistance in the preparation of the samples, and Ms. Zhuang Duan for obtaining some preliminary NMR spectra.

REFERENCES

(1) Goel, A.; Kunnumakkara, A. B.; Aggarwal, B. B. Curcumin as "Curecumin": From kitchen to clinic. *Biochem. Pharmacol.* **2008**, *75*, 787−809.

(2) Esatbeyoglu, T.; Huebbe, P.; Ernst, I. M. A.; Chin, D.; Wagner, A. E.; Rimbach, G. Curcumin − From Molecule to Biological Function. *Angew. Chem., Int. Ed.* **2012**, *51*, 5308−5332.

(3) Gupta, S. C.; Kismali, G.; Aggarwal, B. B. Curcumin, a Component of Turmeric: From Farm to Pharmacy. *BioFactors* **2013**, *39*, 2−13.

(4) Bairwa, K.; Grover, J.; Kania, M.; Jachak, S. M. Recent developments in chemistry and biology of curcumin analogues. *RSC Adv.* **2014**, *4*, 13946−13978.

(5) Cooksey, C. J. Turmeric: old spice, new spice. *Biotech. Histochem.* **2017**, *92*, 309−314.

(6) Sharma, O. P. Antioxidant activity of curcumin and related compounds. *Biochem. Pharmacol.* **1976**, *25*, 1811−1812.

(7) Baum, L.; Ng, A. Curcumin interaction with copper and iron suggests one possible mechanism of action in Alzheimer's disease animal models. *J. Alzheimer's Dis.* **2004**, *6*, 367−377.

(8) Menon, V. P.; Sudheer, A. R. Antioxidant and anti-inflammatory properties of curcumin. In *The Molecular Targets and Therapeutic Uses of Curcumin in Health and Disease*; Aggarwal, B. B., Surh, Y.-J., Shishodia, S., Eds.; Springer: Boston, MA, 2007; pp 105−125.

(9) Salem, M.; Rohani, S.; Gillies, E. R. Curcumin, a promising anticancer therapeutic: a review of its chemical properties, bioactivity and approaches to cancer cell delivery. *RSC Adv.* **2014**, *4*, 10815−10829.

(10) Hewlings, S. J.; Kalman, D. S. Curcumin: A Review of Its' Effects on Human Health. *Foods* **2017**, *6*, 92.

(11) Arablou, T.; Kolahdouz-Mohammadi, R. Curcumin and endometriosis: Review on potential roles and molecular mechanisms. *Biomed. Pharmacother.* **2018**, *97*, 91−97.

(12) Nelson, K. M.; Dahlin, J. L.; Bisson, J.; Graham, J.; Pauli, G. F.; Walters, M. A. The Essential Medicinal Chemistry of Curcumin. *J. Med. Chem.* **2017**, *60*, 1620−1637.

(13) Padmanaban, G.; Nagaraj, V. A. Curcumin May Defy Medicinal Chemists. *ACS Med. Chem. Lett.* **2017**, *8*, 274.

(14) Nelson, K. M.; Dahlin, J. L.; Bisson, J.; Pauli, G. F.; Walters, M. A. Curcumin May (Not) Defy Science. *ACS Med. Chem. Lett.* **2017**, *8*, 467−470.

(15) Bahadori, F.; Demiray, M. A Realistic View on "The Essential Medicinal Chemistry of Curcumin. *ACS Med. Chem. Lett.* **2017**, *8*, 893−896.

(16) Tsuda, T. Curcumin: An Effective or Deceptive Dietary Factor? Challenges for Functional Food Scientists. *J. Agric. Food Chem.* **2018**, *66*, 1059−1060.

(17) Modasiya, M. K.; Patel, V. M. Studies on solubility of curcumin. *Int. J. Pharm. Life Sci.* **2012**, *3*, 1490−1497.

(18) Dev, S.; Prabhakaran, P.; Filgueira, L.; Iyer, K. S.; Raston, C. L. Microfluidic fabrication of cationic curcumin nanoparticles as an anticancer agent. *Nanoscale* **2012**, *4*, 2575−2579.

(19) Sindhu, K.; Rajaram, A.; Sreeram, K. J.; Rajaram, R. Curcumin conjugated gold nanoparticle synthesis and its biocompatibility. *RSC Adv.* **2014**, *4*, 1808−1818.

(20) Sanphui, P.; Goud, N. R.; Khandavilli, U. B. R.; Nangia, A. Fast Dissolving Curcumin Cocrystals. *Cryst. Growth Des.* **2011**, *11*, 4135−4145.

(21) Zabihi, F.; Xin, N.; Jia, J.; Cheng, T.; Zhao, Y. Preparation of Nano-curcumin with Enhanced Dissolution Using Ultrasonic-Assisted Supercritical Anti-solvent Technique. *Int. J. Food Eng.* **2015**, *11*, 609−617.

(22) Reddy, C. A.; Somepalli, V.; Golakoti, T.; Kanugula, A. K.; Karnewar, S.; Rajendiran, K.; Vasagiri, N.; Prabhakar, S.; Kuppusamy, P.; Kotamraju, S.; Kutala, V. K. Mitochondrial-Targeted Curcuminoids: A Strategy to Enhance Bioavailability and Anticancer Efficacy of Curcumin. *PLoS One* **2014**, *9*, e89351.

(23) Garai, A.; Plant, I.; Banerjee, S.; Banik, B.; Kondaiah, P.; Chakravarty, A. R. Photorelease and Cellular Delivery of Mitocurcumin from Its Cytotoxic Cobalt (III) Complex in Visible Light. *Inorg. Chem.* **2016**, *55*, 6027−6035.

(24) Bhattacharyya, U.; Kumar, B.; Garai, A.; Bhattacharyya, A.; Kumar, A.; Banerjee, S.; Kondaiah, P.; Chakravarty, A. R. Curcumin "Drug" Stabilized in Oxidovanadium(IV)-BODIPY Conjugates for Mitochondria-Targeted Photocytotoxicity. *Inorg. Chem.* **2017**, *56*, 12457−12468.

(25) Tønnesen, H. H.; Karlsen, J.; Mostad, A. Structural Studies of Curcuminoids. I. The Crystal Structure of Curcumin. *Acta Chem. Scand.* **1982**, *36*, 475−479.

(26) Parimita, S. P.; Ramshankar, Y. V.; Suresh, S.; Row, T. N. G. Redetermination of curcumin: (1E,4Z,6E)-5-hydroxy-1,7-bis(4-hydroxy-3-methoxy-phenyl)hepta-1,4,6-trien-3-one. *Acta Crystallogr., Sect. E: Struct. Rep. Online* **2007**, *63*, o860−o862.

(27) Sanphui, P.; Goud, N. R.; Khandavilli, U. B. R.; Bhanoth, S.; Nangia, A. New polymorphs of curcumin. *Chem. Commun.* **2011**, *47*, 5013−5015.

(28) Reid, J. W.; Kaduk, J. A.; Garimella, S. V.; Tse, J. S. Rietveld refinement using synchrotron powder diffraction data for curcumin, $C_{21}H_{20}O_6$, and comparison with density functional theory. *Powder Diffr.* **2015**, *30*, 67−75.

(29) Parameswari, A. R.; Devipriya, B.; Jenniefer, S. J.; Muthiah, P. T.; Kumaradhas, P. Low Temperature Crystal Structure of 5-Hydroxy-1,7-Bis-(4-Hydroxy-3-Methoxy-Phenyl)-Hepta-1,6-Dien-3-one. *J. Chem. Crystallogr.* **2012**, *42*, 227−231.

DOI: 10.1021/acs.cgd.8b00859
Cryst. Growth Des. 2018, 18, 5556−5563

(30) Wohlfarth, C. Permittivity (dielectric constant) of liquids. In *CRC Handbook of Chemistry and Physics*; Lide, D. R., Ed.; CRC Press: Boca Raton, FL, 2004−2005; pp 6−155 to 6−177.
(31) Payton, F.; Sandusky, P.; Alworth, W. L. NMR Study of the Solution Structure of Curcumin. *J. Nat. Prod.* **2007**, *70*, 143−146.
(32) Liu, J.; Svärd, M.; Hippen, P.; Rasmuson, Å. C. Solubility and Crystal Nucleation in Organic Solvents of Two Polymorphs of Curcumin. *J. Pharm. Sci.* **2015**, *104*, 2183−2189.
(33) Ukrainczyk, M.; Hodnett, B. K.; Rasmuson, Å. C. Process Parameters in the Purification of Curcumin by Cooling Crystallization. *Org. Process Res. Dev.* **2016**, *20*, 1593−1602.
(34) Thorat, A. A.; Dalvi, S. V. Solid-State Phase Transformations and Storage Stability of Curcumin Polymorphs. *Cryst. Growth Des.* **2015**, *15*, 1757−1770.
(35) Harris, R. K. NMR crystallography: the use of chemical shifts. *Solid State Sci.* **2004**, *6*, 1025−1037.
(36) Gobetto, R. Solid State NMR. In *Making Crystals by Design*; Braga, D., Grepioni, F., Eds.; Wiley-VCH: Weinheim, Germany, 2007; pp 266−292.
(37) Cahill, L. S.; Goward, G. R. Intermolecular Interactions & Structural Motifs. In *NMR Crystallography*; Harris, R. K., Wasylishen, R. E., Duer, M. J., Eds.; Wiley: Chichester, UK, 2009; Chapter 21, pp 305−319.
(38) Potrzebowski, M. J. Organic & Pharmaceutical Chemistry. In *NMR Crystallography*; Harris, R. K., Wasylishen, R. E., Duer, M. J., Eds.; Wiley: Chichester, UK, 2009; Chapter 28, pp 435−453.
(39) Apperley, D. C.; Harris, R. K.; Hodgkinson, P. *Solid-State NMR. Basic Principles & Practice*; Momentum Press: New York, 2012; Chapter 1.4, pp 12−14.
(40) Macholl, S.; Tietze, D.; Buntkowsky, G. NMR crystallography of amides, peptides and protein-ligand complexes. *CrystEngComm* **2013**, *14*, 8627−8638.
(41) Martineau, C.; Senker, J.; Taulelle, F. NMR Crystallography. *Annu. Rep. NMR Spectrosc.* **2014**, *82*, 1−57.
(42) Bryce, D. L. NMR crystallography: structure and properties of materials from solid-state nuclear magnetic resonance observables. *IUCrJ* **2017**, *4*, 350−359.
(43) Brog, J.-P.; Chanez, C.-L.; Crochet, A.; Fromm, K. M. Polymorphism, what it is and how to identify it: a systematic review. *RSC Adv.* **2013**, *3*, 16905−16931.
(44) Zhao, X.-Z.; Jiang, T.; Wang, L.; Yang, H.; Zhang, S.; Zhou, P. Interaction of curcumin with Zn(II) and Cu(II) ions based on experiment and theoretical calculation. *J. Mol. Struct.* **2010**, *984*, 316−325.
(45) Kong, X.; Brinkmann, A.; Terskikh, V.; Wasylishen, R. E.; Bernard, G. M.; Duan, Z.; Wu, Q.; Wu, G. Proton Probability Distribution in the O···H···O Low-Barrier Hydrogen Bond: A Combined Solid-State NMR and Quantum Chemical Computational Study of Dibenzoylmethane and Curcumin. *J. Phys. Chem. B* **2016**, *120*, 11692−11704.
(46) Dunitz, J. D.; Bernstein, J. Disappearing Polymorphs. *Acc. Chem. Res.* **1995**, *28*, 193−200.
(47) Sheldrick, G. M. SHELXT-Integrated space-group and crystal-structure determination. *Acta Crystallogr., Sect. A: Found. Adv.* **2015**, *71*, 3−8.
(48) Sheldrick, G. M. Crystal structure refinement with SHELXL. *Acta Crystallogr., Sect. C: Struct. Chem.* **2015**, *71*, 3−8.
(49) Pines, A.; Gibby, M. G.; Waugh, J. S. Proton-enhanced NMR of dilute spins in solids. *J. Chem. Phys.* **1973**, *59*, 569−590.
(50) Bennett, A. E.; Rienstra, C. M.; Auger, M.; Lakshmi, K. V.; Griffin, R. G. Heteronuclear decoupling in rotating solids. *J. Chem. Phys.* **1995**, *103*, 6951−6958.
(51) Earl, W. L.; VanderHart, D. L. Measurement of ^{13}C Chemical Shifts in Solids. *J. Magn. Reson.* **1982**, *48*, 35−54.
(52) Brouwer, D. H.; Horvath, M. Minimizing the effects of RF inhomogeneity and phase transients allows resolution of two peaks in the ^{1}H CRAMPS NMR spectrum of adamantane. *Solid State Nucl. Magn. Reson.* **2015**, *71*, 30−40.
(53) Taylor, R. E. ^{13}C CP/MAS: Application to Glycine. *Concepts Magn. Reson.* **2004**, *22*, 79−89.
(54) Clark, S. J.; Segall, M. D.; Pickard, C. J.; Hasnip, P. J.; Probert, M. I. J.; Refson, K.; Payne, M. C. First principles methods using CASTEP. *Z. Kristallogr. - Cryst. Mater.* **2005**, *220*, 567−570.
(55) Perdew, J. P.; Burke, K.; Ernzerhof, M. Generalized Gradient Approximation Made Simple. *Phys. Rev. Lett.* **1996**, *77*, 3865−3868.
(56) Perdew, J. P.; Burke, K.; Ernzerhof, M. Generalized Gradient Approximation Made Simple. *Phys. Rev. Lett.* **1997**, *78*, 1396.
(57) Broyden, C. G. The Convergence of a Class of Double-rank Minimization Algorithms. Part I. *J. Inst. Math. Appl.* **1970**, *77*, 76−90.
(58) Broyden, C. G. The Convergence of a Class of Double-rank Minimization Algorithms. Part II. *J. Inst. Math. Appl.* **1970**, *77*, 222−231.
(59) Fletcher, R. A. New Approach to Variable Metric Algorithms. *Comp. J.* **1970**, *13*, 317−322.
(60) Goldfarb, D. A Family of Variable Metric Methods Derived by Variational Means. *Math. Comp.* **1970**, *26*, 23−26.
(61) Shanno, D. F. Conditioning of Quasi-Newton Methods for Function Minimization. *Math. Comp.* **1970**, *24*, 647−657.
(62) Jaffé, H. H.; Orchin, M. In *Theory and Applications of Ultraviolet Spectroscopy*; John Wiley and Sons: New York, 1962; pp 233−235.
(63) Galasso, V.; Kovač, B.; Modelli, A.; Ottaviani, M. F.; Pichierri, F. Spectroscopic and Theoretical Study of the Electronic Structure of Curcumin and Related Fragment Molecules. *J. Phys. Chem. A* **2008**, *112*, 2331−2338.
(64) Khadem Sadigh, M.; Zakerhamidi, M. S.; Shamkhali, A. N.; Babaei, E. Photo-physical behaviors of various active forms of curcumin in polar and low polar environments. *J. Photochem. Photobiol., A* **2017**, *348*, 188−198.
(65) Hibbert, F.; Emsley, J. Hydrogen Bonding and Chemical Reactivity. *Adv. Phys. Org. Chem.* **1990**, *26*, 255−379.
(66) Jeffrey, G. A. In *An Introduction to Hydrogen Bonding*; Oxford University Press: New York, 1997; Chapter 2, pp 11−32.
(67) Steiner, T. The Hydrogen Bond in the Solid State. *Angew. Chem., Int. Ed.* **2002**, *41*, 48−76.
(68) McKenzie, R. H.; Bekker, C.; Athokpam, B.; Ramesh, S. G. Effect of quantum nuclear motion on hydrogen bonding. *J. Chem. Phys.* **2014**, *140*, 174508.
(69) Emsley, J. The composition, structure and hydrogen bonding of the β-diketones. In *Struct. Bonding (Berlin)*; Emsley, J., Ernst, R. D., Hathaway, B. J., Warren, K. D., Eds.; Springer: Berlin Heidelberg, 1984; Vol. *57*, pp 147−191.
(70) Gilli, G.; Bellucci, F.; Ferretti, V.; Bertolasi, V. Evidence of Resonance-Assisted Hydrogen Bonding from Crystal-Structure Correlations on the Enol Form of the β-Diketone Fragment. *J. Am. Chem. Soc.* **1989**, *111*, 1023−1028.
(71) Gilli, P.; Bertolasi, V.; Pretto, L.; Ferretti, V.; Gilli, G. Covalent versus Electrostatic Nature of the Strong Hydrogen Bond: Discrimination among Single, Double, and Asymmetric Single-Well Hydrogen Bonds by Variable-Temperature X-ray Crystallographic Methods in β-Diketone Enol RAHB Systems. *J. Am. Chem. Soc.* **2004**, *126*, 3845−3855.
(72) Grabowski, S. J. What Is the Covalency of Hydrogen Bonding? *Chem. Rev.* **2011**, *111*, 2597−2625.
(73) Pople, J. A.; Beveridge, D. L. In *Approximate Molecular Orbital Theory*; McGraw-Hill Book Company: New York, 1970; Chapter 4, pp 110−113.
(74) Fleischer, E. B.; Sung, N.; Hawkinson, S. The Crystal Structure of Benzophenone. *J. Phys. Chem.* **1968**, *72*, 4311−4312.
(75) Larsen, N. W. Microwave Spectra of the Six Mono-^{13}C-Substituted Phenols and of Some Monodeuterated Species of Phenol. Complete Substitution Structure and Absolute Dipole Moment. *J. Mol. Struct.* **1979**, *51*, 175−190.
(76) Tsuzuki, S.; Houjou, H.; Nagawa, Y.; Hiratani, K. High-Level ab Initio Calculations of Torsional Potential of Phenol, Anisole, and *o*-Hydroxyanisole: Effects of Intramolecular Hydrogen Bond. *J. Phys. Chem. A* **2000**, *104*, 1332−1336.

DOI: 10.1021/acs.cgd.8b00859
Cryst. Growth Des. 2018, 18, 5556−5563

(77) Dorofeeva, O. V.; Shishkov, I. F.; Karasev, N. M.; Vilkov, L. V.; Oberhammer, H. Molecular structures of 2-methoxyphenol and 1,2-dimethoxybenzene as studied by gas-phase electron diffraction and quantum chemical calculations. *J. Mol. Struct.* **2009**, *933*, 132−141.
(78) Siskos, M. G.; Choudhary, M. I.; Gerothanassis, I. P. Hydrogen Atomic Positions of O-H···O Hydrogen Bonds in Solution and in the Solid State: The Synergy of Quantum Chemical Calculations with ^{1}H-NMR Chemical Shifts and X-ray Diffraction Methods. *Molecules* **2017**, *22*, 415.
(79) Berglund, B.; Vaughan, R. W. Correlations between proton chemical shift tensors, deuterium quadrupole couplings, and bond distances for hydrogen bonds in solids. *J. Chem. Phys.* **1980**, *73*, 2037−2043.
(80) Kaliaperumal, R.; Sears, R. E. J.; Ni, Q. W.; Furst, J. E. Proton chemical shifts in some hydrogen bonded solids and a correlation with bond lengths. *J. Chem. Phys.* **1989**, *91*, 7387−7391.
(81) Bertolasi, V.; Gilli, P.; Ferretti, V.; Gilli, G. Intramolecular O-H···O hydrogen bonds assisted by resonance. Correlation between crystallographic data and ^{1}H NMR chemical shifts. *J. Chem. Soc., Perkin Trans. 2* **1997**, *2*, 945−952.
(82) Siskos, M. G.; Choudhary, M. I.; Gerothanassis, I. P. Refinement of labile hydrogen positions based on DFT calculations of ^{1}H NMR chemical shifts: comparison with X-ray and neutron diffraction methods. *Org. Biomol. Chem.* **2017**, *15*, 4655−4666.
(83) Harris, R. K.; Jackson, P.; Merwin, L. H.; Say, B. J.; Hägele, G. Perspectives in High-resolution Solid-state Nuclear Magnetic Resonance, with Emphasis on Combined Rotation and Multiple-pulse Spectroscopy. *J. Chem. Soc., Faraday Trans. 1* **1988**, *1* (84), 3649−3672.
(84) Emmler, Th.; Gieschler, S.; Limbach, H. H.; Buntkowsky, G. A simple method for characterization of OHO-hydrogen bonds by ^{1}H-solid state NMR spectroscopy. *J. Mol. Struct.* **2004**, *700*, 29−38.
(85) Jeffrey, G. A.; Yeon, Y. The Correlation Between Hydrogen-Bond Lengths and Proton Chemical Shifts in Crystals. *Acta Crystallogr., Sect. B: Struct. Sci.* **1986**, *B42*, 410−413.
(86) Péret-Almeida, L.; Cherubino, A. P. F.; Alves, R. J.; Dufossé, L.; Glória, M. B. A. Separation and determination of the physico-chemical characteristics of curcumin, demethoxycurcumin and bisdemethoxycurcumin. *Food Res. Int.* **2005**, *38*, 1039−1044.
(87) Kiuchi, F.; Goto, Y.; Sugimoto, N.; Akao, N.; Kondo, K.; Tsuda, Y. Nematocidal Activity of Turmeric: Synergistic Action of Curcuminoids. *Chem. Pharm. Bull.* **1993**, *41*, 1640−1643.
(88) Liddel, U.; Ramsey, N. F. Temperature Dependent Magnetic Shielding in Ethyl Alcohol. *J. Chem. Phys.* **1951**, *19*, 1608.
(89) Arnold, J. T.; Packard, M. E. Variations in Absolute Chemical Shift of Nuclear Induction Signals of Hydroxyl Groups of Methyl and Ethyl Alcohol. *J. Chem. Phys.* **1951**, *19*, 1608−1609.
(90) Muller, N.; Reiter, R. C. Temperature Dependence of Chemical Shifts of Protons in Hydrogen Bonds. *J. Chem. Phys.* **1965**, *42*, 3265−3269.
(91) Grzesiek, S.; Becker, E. D. Hydrogen Bonding. *eMagRes.* **2011**, DOI: 10.1002/9780470034590.emrstm0216.pub2.
(92) Modig, K.; Halle, B. Proton Magnetic Shielding Tensor in Liquid Water. *J. Am. Chem. Soc.* **2002**, *124*, 12031−12041.

DOI: 10.1021/acs.cgd.8b00859
Cryst. Growth Des. 2018, 18, 5556−5563